Evidence for Family-Meakin Dynamical Scaling in Island Growth and Coalescence during Vapor Phase Deposition

Leyla Çolakerol Arslan,* Christopher Sanborn, Eitan Anzenberg, and Karl F. Ludwig, Jr.
Department of Physics, Boston University, Boston, Massachusetts 01770, USA
(Received 11 February 2012; revised manuscript received 23 July 2012; published 7 September 2012)

Using real-time grazing-incidence small-angle x-ray scattering, we find that the processes of island formation and coalescence during the room-temperature vapor phase deposition of aluminum lead to dynamical scaling of the evolving surface morphology. The scaling is quantitatively consistent with the self-similarity predicted by the Family-Meakin model, which was developed to describe *liquid* droplet deposition, growth, and coalescence. The Family-Meakin model assumes only that atomic diffusion over the substrate between islands or droplets is negligible and that diffusion between impinging islands or droplets is sufficient to give complete coalescence. Therefore the dynamical scaling morphology evolution identified here may be common in the initial stages of those solid film growth processes which proceed by island formation and growth.

DOI: 10.1103/PhysRevLett.109.106102 PACS numbers: 81.15.Aa, 61.05.cf, 68.55.−a

Materials growth processes at surfaces are at the core of widely used technologies; understanding the detailed morphological evolution during such growth becomes ever more important as technologically desirable film thicknesses decrease. Film growth by vapor phase deposition on an incompatible substrate typically begins with island formation and growth and proceeds with impingement and coalescence into a continuous film. Such film growth can be simulated with atomistic models which usually have no analytical solution; for a given set of parameters, numerical results can be obtained through simulations. We show here, however, that island growth and coalescence can drive the evolving surface morphology to a well-defined and easily visualized dynamical scaling regime identified in theory and simulations by Family and Meakin (FM) [1] for *liquid* droplet deposition, growth, and evolution. The FM model shows that these processes lead to a dynamical self-similarity and scaling of the droplet size distribution. For the homogeneous random deposition of small droplets, the model gives a bimodal distribution of droplet sizes, with a broad distribution of smaller droplets situated between a relatively monodisperse set of larger droplets. These large droplets form and coarsen because of impingement and coalescence events. The FM model assumes that there is no diffusion between droplets; all evolution is driven by the deposition process itself. When two droplets impinge, however, they immediately coalesce to form a larger droplet of the same overall shape (presumably a spherical cap in the case of many three-dimensional liquid droplets). Our investigation of early-stage room-temperature aluminum film growth on two separate oxide surfaces takes advantage of real-time grazing-incidence small-angle x-ray scattering (GISAXS) to follow the surface morphology kinetics during growth and kinetic Monte Carlo simulations to make detailed comparison of the GISAXS results with FM model predictions.

These experiments utilized a facility constructed on beam line X21 of the National Synchrotron Light Source of Brookhaven National Laboratory for the *in situ* study of surface and thin films processes. It utilizes a chamber with a base pressure below 10^{-9} torr. For these experiments an effusion cell was used for thermal Al film growth on substrates of native silicon oxide on Si(111) and on sapphire (0001). The deposition flux was varied by using effusion cell temperatures of 1030 and 1050 °C, and all depositions were performed with the substrate at room temperature. Growth rates used here were very low to carefully examine the early-stage kinetics. Estimates based on the GISAXS results presented below, *post facto* atomic force microscopy (AFM), vapor pressure calculations, and comparison with simulations suggest that the growth rate for an effusion cell temperature of 1050 °C was approximately 0.73 nm/min and the growth rate for a cell temperature of 1030 °C was approximately 34% slower. The GISAXS measurements during deposition used a photon energy of 10 keV and a linear pixel detector with pattern readout approximately every 1.06 s. The real-time growth scans used an incident x-ray angle of 0.8° and the exit angle was 0.2°, near the critical angle for total reflection; these scans primarily study in-plane order. Immediately following each deposition run, the incident angle was scanned to examine the scattering in a direction nearly perpendicular to the surface—designated the q_z direction in reciprocal space. These yield information about the height of surface structures. Although the surface scattering is enhanced by use of a grazing exit angle, distorted-wave Born approximation calculations using the ISGISAXS program [2,3] show that, to sufficient accuracy, the scattering is proportional to the structure factor calculated within the simpler Born approximation using an effective q_z that takes into account refraction in the material. For the real-time GISAXS scans this gives an effective

$q_z \cong 0.7$ nm^{-1}. When the height h of structures on the surface is small, such that $q_z h \leq 1$, the real-time GISAXS scans effectively measure the evolving height-height correlation function $S(q_\parallel, t)$ on the surface, where $q_\parallel$ is the in-plane wave number [4]. When surface roughness grows higher, the q_z dependence of the scattering must be taken into account when quantitatively interpreting the real-time results.

Figure 1 shows a typical evolution of the GISAXS pattern during Al deposition on native silicon oxide at an effusion cell temperature of 1050 °C. An unchanging background from the tail of the specular peak centered at $q_\parallel = 0$ has been subtracted from each scan. In the figure, it is observed that a peak due to nanoscale correlations forms in the structure factor; it rapidly coarsens, decreasing in wave number and growing in amplitude. This directly shows the formation and evolution of correlated nanoscale structures on the surface during growth. As discussed below, the GISAXS peak position shows that these have characteristic length scales that typically grow from ~2 to ~10 nm during the time of the experiment. Following closure of the effusion cell shutter during the real-time studies, the evolution of the GISAXS scattering pattern abruptly slows; the correlation peak continues to grow for approximately 10 s after the shutter closure but then changes only little on the time scales that could be readily observed (1 h) *in situ* at the synchrotron. Thus on these time scales the kinetics of the Al island evolution is largely driven by the deposition process, but apparently with a smaller relaxational component as well. This is contrary to the uninterrupted coarsening expected for an Ostwald ripening process in which atoms diffuse from small islands to large islands, driven by the difference in free energy and independent of deposition. However, as elucidated below, the behavior is exactly what is expected from the processes of island growth and coalescence.

A *post facto* AFM image taken after 85 s of deposition with a 1050 °C effusion cell temperature after removal from the *in situ* growth chamber is shown in the inset in Fig. 1. Exposure of a surface Al layer to air results in its oxidation, and significant Ostwald ripening on longer time scales than the *in situ* investigations here may occur between the x-ray experiments and the *ex situ* AFM, but the AFM images clearly show the formation of three-dimensional islands on the surface; the correlations in the GISAXS structure factor are due to correlations between these growing islands. Moreover, the morphology observed, with small islands interspersed between large islands, is characteristic of that associated with droplets in the FM theory.

To characterize the evolving surface morphology during growth, the real-time GISAXS data were first fit to Gaussian line shapes to extract the peak position $q_{\max}(t)$ and peak height $S_{\max}(t)$. Comparison of surface evolution as a function of deposition rate (1050 versus 1030 °C effusion cell temperature) and surface (sapphire versus native silicon oxide) shows that, for these ranges of parameters, the morphology evolution simply scales with deposition fluence and is independent of which of the two substrates is used. This can be seen in Fig. 2, which shows the increase in characteristic in-plane length scale between islands $R(t) = 2\pi/q_{\max}(t)$ plotted as a function of deposition fluence $F =$ (deposition rate) × (time). As can be seen, following an initial time period during which the peak is outside the window of the detector, the characteristic in-plane length scale $R(t)$ grows linearly in fluence.

The final heights of the islands on the surface can be determined from the q_z scans taken at the end of each deposition run. As an example, Fig. 3 shows the q_z scan at the $S_{\max}$ in-plane peak position following 85 s of deposition onto the silicon oxide at 1050 °C effusion cell temperature. A simple fit with a spherical cap structure factor yields an island height of about 3 nm. This is a substantial fraction of the characteristic distance between islands at this point ($R \cong 7$ nm) and suggests that the islands are strongly three-dimensional. Other samples give similar results.

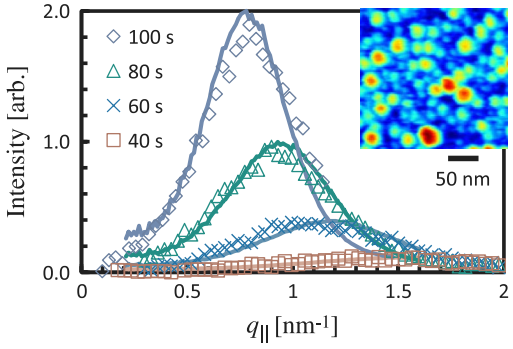

FIG. 1 (color online). Evolution of GISAXS scattering patterns during room-temperature Al deposition on native oxide of Si. The effusion cell temperature was 1050 °C. The lines are FM simulations. The inset shows a *post facto* AFM topograph after 240 s deposition at 1050 °C effusion cell temperature. The color z range spans 4.5 nm.

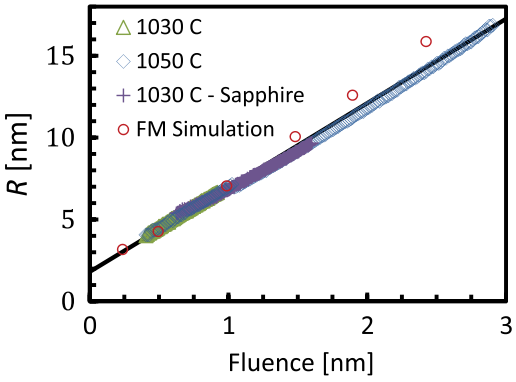

FIG. 2 (color online). Evolution of characteristic in-plane length scale R as a function of fluence, showing collapse onto a common linear growth for deposition onto native oxide of Si(100) at effusion cell temperatures of 1050 and 1030 °C and deposition onto a sapphire substrate at 1030 °C.

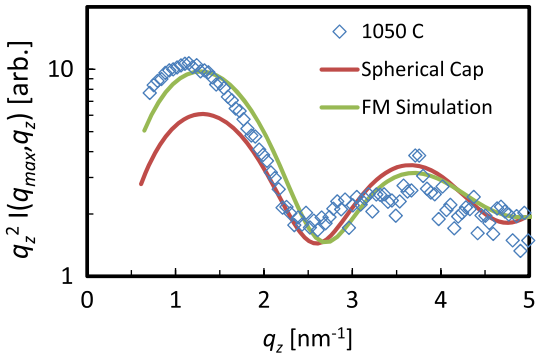

FIG. 3 (color online). Weighted q_z scan following 85 s of Al deposition using an effusion cell temperature of 1050 °C. The red line shows a fit to the structure factor of a spherical cap of height 3 nm; the green line shows results from a FM simulation.

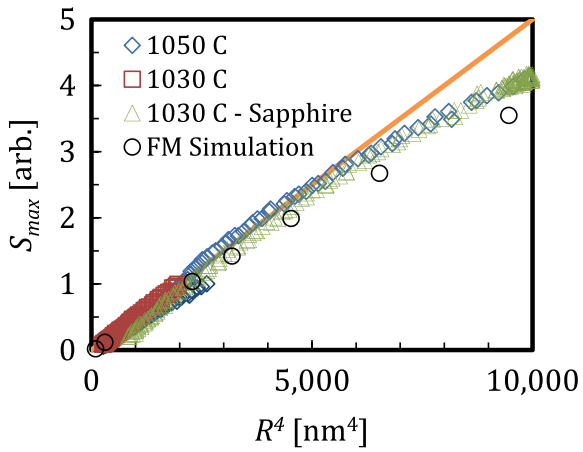

FIG. 4 (color online). Dependence of peak intensity $S_{\max}$ on characteristic in-plane distance R showing $S_{\max} \sim R^4$ at small R (early times) but deviating for large R (and therefore large island heights) because of destructive interference between the bottom and top of the islands.

The primacy of deposition in driving surface evolution and the formation of well-defined droplet shapes are hallmarks of the FM model of droplet growth and coarsening. For homogeneous three-dimensional droplet or island formation and coalescence on a two-dimensional surface, the model predicts that the characteristic length scale should grow linearly in time, in accord with the $R(t)$ results of Fig. 2. Moreover, as noted above, the final surface morphologies as seen by AFM exhibit the characteristic morphology demonstrated by the model for homogeneous droplet nucleation. To do more detailed comparisons, we used kinetic Monte Carlo simulations of the FM model to examine how its structure factor evolves. As might be expected, a peak grows in the model structure factor and coarsens with time. The peak position is indicative of the characteristic distance between the relatively monodisperse large droplets. The line curves in Fig. 1 are calculated structure factors from a FM simulation, showing excellent agreement with the observed GISAXS evolution, particularly at early times. The simulations presented in this Letter used an initial FM droplet radius $r_0 = 0.475$ nm and a contact angle near 90°, so that the islands are essentially modeled as hemispheres. This produces the correct evolution of the characteristic length scale $R(t)$ (circles in Fig. 2) and also the correct final characteristic height of the islands as seen in the q_z scan (Fig. 3).

In the FM model, the in-plane correlation peak maximum $S_{\max}$ is proportional to NMn^2, where N is the number of islands or droplets, M is the average number of correlated neighbors around each island or droplet, and n^2 is the average of the square number of atoms in each droplet. Because of the self-similarity of the island and droplet morphology evolution, M is constant and all length scales increase with the same time dependence as $R(t)$, the characteristic distance between large islands. Thus the mean diameter of the large islands $D(t)$ is simply proportional to $R(t)$; in the simulations $R(t) \cong 1.075\, D(t)$. The number of atoms in each large droplet increases as $n \sim D^3 \sim R^3$. Individual drops grow until they impinge on neighbors and become subsumed through the coalescence process. The number of large islands or droplets decreases as $N \sim 1/R^2$ [5]. Therefore the in-plane correlation peak maximum $S_{\max}$ grows as $NMn^2 \sim R^4$. Comparing this prediction to the real-time GISAXS results is complicated by the nonzero q_z required for the experiment. We can expect *a priori* that the predicted behavior would be observed for small R (i.e., early times) but that the observed growth in correlation peak amplitude would slow with increasing R (and hence increasing island height) because of destructive interference between scattering from the bottoms of the islands and the tops. Indeed, this is exactly what is observed in Fig. 4. [6] Moreover, structure factor calculations from FM simulations *using the q_z value of the experiment* show the same trend as the experimental results (circles in Fig. 4).

A distinctive property of the FM model is that the droplet size distribution exhibits dynamical scaling due to self-similarity between typical droplet patterns at one point in time and spatially scaled droplet patterns later. The distribution of islands of length scale r varies as $N(r) = G(r/R(t))$, where G is a scaling function discussed in Ref. [1]. The scaling of the island distribution function suggests that the height-height structure factor should also exhibit dynamical scaling $S(q, t) = R(t)^4 g(qR(t))$, where g is again a scaling function. We have confirmed that this is the case with the FM simulations. For the real-time GISAXS data, Fig. 5 shows that, at early times in the island and growth process, the structure factors do exhibit the FM dynamical scaling. Both the observed and the FM structure factors are slightly asymmetric, with longer tails on the high-q side, though the asymmetry is more pronounced in the experimental structure factors. At later times the nonzero q_z of the real-time data prevents such a simple comparison.

In considering why the Al island growth and coalescence follows FM dynamics so well, it is notable that the *post facto* AFM topographs suggest that there is sufficient diffusion

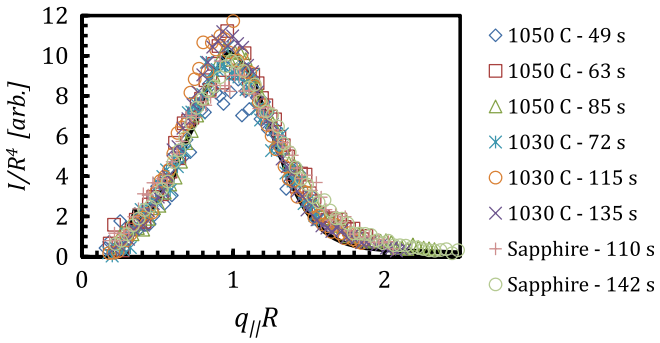

FIG. 5 (color online). Dynamical scaling of the real-time GISAXS structure factor, showing collapse onto a common line shape. The black line is the scaling structure factor from FM simulations.

within each island to allow it to assume a compact shape, decreasing surface energy. At room temperature, the bulk self-diffusion coefficient of Al is of the order of 10^{-23} cm^2/s [7–10], so that bulk diffusion in the Al is negligible on the time scales of interest. Estimates of Al surface diffusion coefficients vary widely depending, for instance, on the crystalline face [11–13]. However, reported surface diffusion coefficients on polycrystalline films at room temperature are in the range of 10^{-12} cm^2/s [14]. Thus, Al atoms could diffuse across the surfaces of the islands seen here in of the order of 10 s, leading to the compact shapes observed.

While the FM model assumes the deposition of small droplets, vapor phase deposition from an effusion cell instead deposits individual atoms. We have performed simple simulations of atom deposition and immediate migration either to existing islands or to form new islands. The initial distance between islands is typically about twice the distance over which atoms migrate. If the atomistic simulations include no diffusion between atoms in existing islands, and immediate coalescence of islands, then the island morphology quickly comes to resemble that found in the original FM model. Thus the deposition of individual atoms instead of droplets does not change the kinetics beyond the original island formation stage.

The geometry of these experiments limited the maximum $q_{\|}$ accessible to about 2 nm^{-1}, so that it was not possible to effectively analyze data at the earliest times when islands were closer together than $2\pi/(2\ \text{nm}^{-1}) \sim 3$ nm. The correlation peak is observed to move into the detector from higher wave number, not grow initially at a wave number on the detector, so the initial islands forming during deposition are less than 3 nm apart. We can estimate the initial size of islands when they first form, however, by extrapolating the characteristic length scale shown in Fig. 2 back to the beginning of the deposition process. This gives $R(F = 0) \cong 2$ nm, suggesting that the distance over which adatoms move on the bare surface to join existing islands or to nucleate new ones is $\sim$1 nm. The value of initial droplet size $r_0 = 0.475$ nm chosen for the FM simulations is in accord with these length scales.

Given the simple assumptions of the FM model—rapid coalescence of islands to a consistent shape upon impingement and insignificant diffusion between islands—the behavior observed here may be common during the initial stages of those thin solid film growth processes that proceed by island formation, growth, and coalescence. The duration of the growth period during which the FM model will be quantitatively useful, however, will likely be constrained by the decreasing ability of islands to coalesce into a compact shape by atomic diffusion as the characteristic island size increases.

This work was supported by the U.S. DOE Office of Science, Office of Basic Energy Sciences under DE-FG02-03ER46037. Use of the NSLS was supported by the U.S. DOE, Office of Science, Office of Basic Energy Sciences, under Contract No. DE-AC02-98CH10886.

*Present address: Department of Physics, Gebze Institute of Technology, Kocaeli, 41400 Turkey.

[1] F. Family and P. Meakin, Phys. Rev. A **40**, 3836 (1989); Phys. Rev. Lett. **61**, 428 (1988); Rep. Prog. Phys. **55**, 157 (1992).
[2] R. Lazzari, F. Leroy, and G. Renaud, Phys. Rev. B **76**, 125411 (2007).
[3] R. Lazzari, J. Appl. Crystallogr. **35**, 406 (2002).
[4] S. K. Sinha, E. B. Sirota, S. Garoff, and H. B. Stanley, Phys. Rev. B **38**, 2297 (1988).
[5] As discussed in the papers of Ref. [1], the *total* number of droplets is dominated by the behavior of the continuous distribution of small droplets and decreases as $t^{-0.26}$ for three-dimensional droplets on a two-dimensional surface. However, the number of large droplets decreases as t^{-2}, as can be seen from integrating the appropriate parts of Eqs. (5) and (6) in the first paper of Ref. [1].
[6] This comparison requires scaling the intensity for each sample by a single multiplicative factor. Such correction is to be expected since the exact sample shape, and therefore the illuminated volume in the x-ray beam, varies from sample to sample.
[7] F. Fradin and T. Rowland, Appl. Phys. Lett. **11**, 207 (1967).
[8] J. Burke and T. Ramachandran, Metall. Trans. **3**, 147 (1972).
[9] P. Agrawal, B. Rice, and D. Thompson, Surf. Sci. **515**, 21 (2002).
[10] D. Liu, L. Zhang, Y. Du, H. Xu, S. Liu, and L. Liu, CALPHAD: Comput. Coupling Phase Diagrams Thermochem. **33**, 761 (2009).
[11] H. Huang, G. Gilmer, and T. Díaz de la Rubia, J. Appl. Phys. **84**, 3636 (1998).
[12] J. Barth, H. Brune, B. Fischer, J. Weckesser, and K. Kern, Phys. Rev. Lett. **84**, 1732 (2000).
[13] N. Papanicolaou, V. C. Papathanakos, and D. G. Papageorgiou, Physica (Amsterdam) **296B**, 259 (2001).
[14] T. S. Cale, M. K. Jain, D. S. Taylor, R. L. Duffin, and C. J. Tracy, J. Vac. Sci. Technol. **11**, 311 (1993); D. S. Taylor, M. K. Jain, and T. S. Cale, J. Vac. Sci. Technol. A **16**, 3123 (1998).